# *Evaluation of sampling methods for fracture network characterization using outcrops*

**Conny Zeeb, Enrique Gomez-Rivas, Paul D. Bons, and Philipp Blum**

## ABSTRACT

Outcrops provide valuable information for the characterization of fracture networks. Sampling methods such as scanline sampling, window sampling, and circular scanline and window methods are available to measure fracture network characteristics in outcrops and from well cores. These methods vary in their application, the parameters they provide and, therefore, have advantages and limitations. We provide a critical review on the application of these sampling methods and apply them to evaluate two typical natural examples: (1) a large-scale satellite image from the Oman Mountains, Oman (120,000 $m^2$ [1,291,669 $ft^2$]), and (2) a small-scale outcrop at Craghouse Park, United Kingdom (19 $m^2$ [205 $ft^2$]). The differences in the results emphasize the importance to (1) systematically investigate the required minimum number of measurements for each sampling method and (2) quantify the influence of censored fractures on the estimation of fracture network parameters. Hence, a program was developed to analyze 1300 sampling areas from 9 artificial fracture networks with power-law length distributions. For the given settings, the lowest minimum number of measurements to adequately capture the statistical properties of fracture networks was found to be approximately 110 for the window sampling method, followed by the scanline sampling method with approximately 225. These numbers may serve as a guideline for the analyses of fracture populations with similar distributions. Furthermore, the window sampling method proved to be the method that is least sensitive to censoring bias. Reevaluating our natural examples with the window sampling method showed that the



Manuscript received March 6, 2012; provisional acceptance July 23, 2012; revised manuscript received December 18, 2012; final acceptance February 13, 2013.
DOI:10.1306/02131312042

## AUTHORS

Conny Zeeb ~ *Karlsruhe Institute of Technology, Institute for Applied Geosciences, Kaiserstrasse 12, 76131 Karlsruhe, Germany; present address: Geotechnical Institute, TU Bergakademie Freiberg, Gustav-Zeuner-Straße 1, 09596 Freiberg, Germany; conny.zeeb@ifgt.tu-freiberg.de*

Conny Zeeb is a Ph.D. student at the University of Tübingen where he worked on the characterization of fracture networks and on the simulation of fluid transport in fractured rocks. Since 2013, he has been a scientific assistant at the University of Freiberg. His current research focuses on hydraulic fracturing and coupled thermo-hydro-mechanical processes.

Enrique Gomez-Rivas ~ *University of Tübingen, Department of Geosciences, Wilhelmstrasse 56, 72074 Tübingen, Germany; enrique.gomez-rivas@uni-tuebingen.de*

Enrique Gomez-Rivas is a postdoctoral research fellow at the University of Tübingen. He received his Ph.D. in structural geology from the Autonomous University of Barcelona, Spain. His research interests mainly focus on the formation of fractures and other tectonic structures as well as on fluid-rock interaction (fluid flow and dolomitization), integrating field studies with numerical modeling.

Paul D. Bons ~ *University of Tübingen, Department of Geosciences, Wilhelmstrasse 56, 72074 Tübingen, Germany; paul.bons@uni-tuebingen.de*

Paul Bons is currently a professor in the Department of Geosciences where he leads the Structural Geology Group. His research covers the formation of veins, fluid flow, and the formation of deformation structures, in particular, through numerical modeling. He received his doctoral degree from Utrecht University, Netherlands, and worked at Monash University, Melbourne, Australia, and at Mainz University, Germany.

Philipp Blum ~ *Karlsruhe Institute of Technology, Institute for Applied Geosciences, Kaiserstrasse 12, 76131 Karlsruhe, Germany; philipp.blum@kit.edu*

Philipp Blum is currently an associate professor for engineering geology at the Karlsruhe Institute of Technology. Previously, he was an

assistant professor at the University of Tübingen. In 2003, he completed his Ph.D. at the University of Birmingham. From 2003 to 2005 he worked for United Research Services Germany. His current research interests are on coupled THMC processes in porous and fractured rocks.

## ACKNOWLEDGEMENTS

This study was conducted within the framework of Deutsche Wissenschaftliche Gesellschaft für Erdöl, Erdgas und Kohle e.V. (German Society for Petroleum and Coal Science and Technology) research project 718 "Mineral Vein Dynamics Modeling," which is funded by the companies ExxonMobil Production Deutschland GmbH, Gaz de France SUEZ E&P Deutschland GmbH, Rheinisch-Westfälische Elektrizitätswerk Dea AG, and Wintershall Holding GmbH, within the basic research program of the Wirtschaftsverband Erdöl und Erdgasgewinnung e.V. We thank the companies for their financial support, their permission to publish these results, and funding of a Ph.D. grant to Conny Zeeb and a postdoctoral grant to Enrique Gomez-Rivas. We also thank Janos Urai and Marc Holland from the Rheinisch-Westfaelische Technische Hochschule Aachen for permission to use their remote sensing data from the Oman Mountains, Oman. We thank Tricia F. Allwardt, Alfred Lacazette, and an anonymous reviewer and the AAPG editorial board for their helpful reviews and suggestions. The AAPG Editor thanks the following reviewers for their work on this paper: Tricia F. Allwardt, Alfred Lacazette, and an anonymous reviewer.

existing percentage of censored fractures significantly influences the accuracy of inferred fracture network parameters.

## INTRODUCTION

Fractures and other mechanical discontinuities act as preferential fluid pathways in the subsurface, thus strongly controlling fluid flow in hydrocarbon reservoirs. An essential step for reservoir characterization is the acquisition of fracture network data and the subsequent upscaling of their statistical properties (Long et al., 1982; Jackson et al., 2000; Blum et al., 2009). Because terminology for mechanical defects in rocks is diverse and commonly has genetic connotations, we also include joints and veins when using the term "fractures." A common method to evaluate the degree of fracturing in the subsurface is the characterization of fracture networks from outcropping subsurface analogs, well cores, or image logs (Dershowitz and Einstein, 1988; Priest, 1993; National Research Council, 1996; Mauldon et al., 2001; Bour et al., 2002; Laubach, 2003; Blum et al., 2007; Jing and Stephansson, 2007; Guerriero et al., 2011). This process includes the acquisition of geometric data from fractures and its subsequent analysis to find statistical distributions and relationships between parameters (Einstein and Baecher, 1983; Priest 1993; Blum et al., 2005; Barthélémy et al., 2009; Tóth, 2010; Tóth and Vass, 2011). The most widely used acquisition methods for fracture network statistical parameters are (1) scanline sampling (Priest and Hudson, 1981; LaPointe and Hudson, 1985; Priest 1993), (2) window sampling (Pahl, 1981; Priest, 1993), and (3) circular scanline and window (or "circular estimator") methods (Mauldon et al., 2001; Rohrbaugh et al., 2002) (Figure 1).

In the subsurface, fracture sampling is constrained to boreholes, which basically corresponds to scanline sampling. Well cores and image logs provide valuable in-situ information on, for example, fracture spacing, orientation, aperture, and cementation (e.g., Olson et al., 2009). However, fracture sampling strongly depends on borehole inclination. Fracture intersection frequency is highest for a borehole perpendicular to the fractures of a set, whereas if the borehole is parallel to the fracture set, sampling is very limited, and no or only few data can be acquired. Some parameters, such as average fracture spacing (Narr, 1996), can be estimated irrespective of borehole inclination. Ortega and Marrett (2000) showed that an extrapolation of fracture frequencies from the microscopic scale to the macroscopic scale is possible up to the scale of mechanical layering. However, it is impossible to directly measure

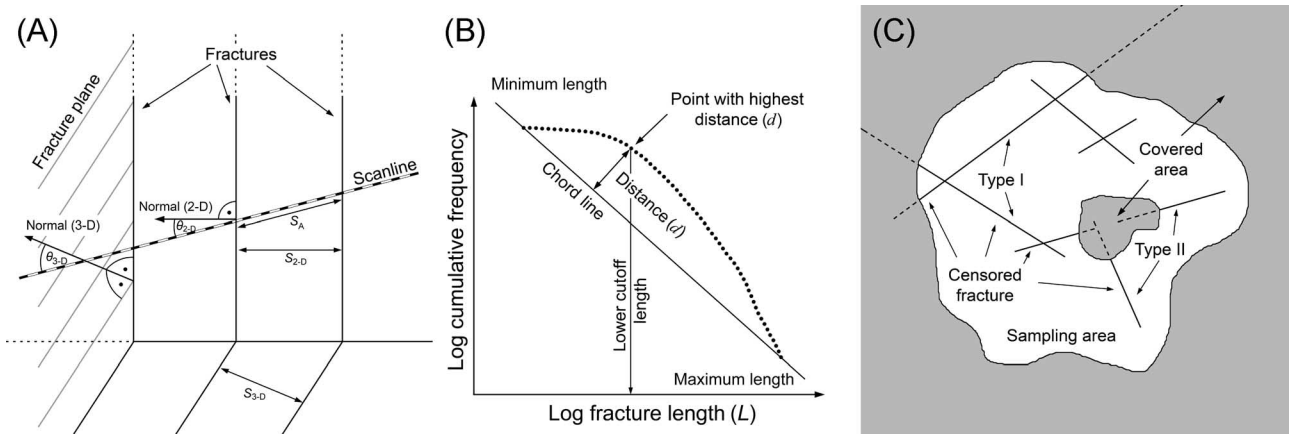


**Figure 1.** (A) Sketch illustrating orientation bias and the definition of the variables required to calculate the factor for the Terzaghi correction (equation 1). $S_A$ is the apparent spacing measured along a scanline, $S_{2\text{-}D}$ is the true spacing between two fracture traces, and $S_{3\text{-}D}$ is the true spacing between two fracture planes. $\theta_{2\text{-}D}$ and $\theta_{3\text{-}D}$ are the angles between the normal to a fracture trace or a fracture plane, respectively, and a scanline. (B) Illustration of the chord method (Pérez-Claros et al., 2002; Roy et al., 2007). In a log-log plot of fracture length against cumulative frequency, the line through the data point with the shortest length and the data point with the longest length is calculated. The fracture length from the data point with the highest distance $d$ to this line is used as the lower cutoff for the truncation bias. (C) Censoring bias caused by the boundaries of a sampling area (type I) and covered parts in an outcrop (type II).

fracture lengths in the subsurface, which is crucial for fluid-flow modeling and the evaluation of an equivalent permeability in subsurface reservoirs (e.g., Philip et al., 2005). Although scaling relationships between the apertures and lengths for opening-mode fractures have been reported (e.g., Olson, 2003; Scholz, 2010), the exact nature of these relationships is still under debate (e.g., Olson and Schultz, 2011). Furthermore, to our knowledge, scaling relationships for fractures in layered rocks have not been systematically investigated yet. Thus, the analysis of outcropping subsurface analogs can provide valuable additional information, especially on fracture length distributions for the simulation of fluid flow in subsurface reservoirs (e.g., Belayneh et al., 2009).

Each of the three sampling methods mentioned above has advantages and limitations when applied to an outcrop. Previous studies by Rohrbaugh et al. (2002), Weiss (2008), Belayneh et al. (2009), and Manda and Mabee (2010) provide information concerning the application of the scanline sampling, window sampling, and circular estimator methods for specific case studies. However, a comprehensive analysis including (1) the application of all three sampling methods to the same case; (2) their verification using artificial fracture networks (AFNs) with known input parameters; and (3) the use of a power law to describe the distribution of fracture lengths, which is commonly reported for natural fracture networks (e.g., Pickering et al., 1995; Odling 1997; Bonnet et al., 2001; Blum et al., 2005; Tóth, 2010; LeGarzic et al., 2011), is still lacking. A main issue here is the lack of a general consensus regarding the minimum number of length measurements required to adequately determine the length distribution of a fracture network. According to Priest (1993) the sampling area should contain between 150 and 300 fractures, of which approximately 50% should have at least an end visible. Furthermore, Bonnet et al. (2001) suggested the sampling of a minimum of 200 fractures to adequately define exponents of power-law length distributions. However, these numbers only apply to specific case studies. Accordingly, the minimum number of fractures a sampling area should contain to apply the scanline sampling, window sampling, or circular estimator methods are not unequivocally defined yet. A systematic study evaluating this issue is therefore needed.

A topic concerning the measurement of fracture networks in outcrops is the actual influence of censored fractures on network parameter estimates. Correcting censoring bias is a challenging task and relies on certain assumptions of fracture shape (e.g., disc, ellipsoid, or rectangle) and fracture

**Table 1.** Additional Important Fracture Parameters, Necessary to Adequately Simulate Fluid Flow Through Fractured Rocks, and Definitions of Fracture Size

| Parameter | Definition |
|---|---|
| Filling | The filling of the fracture void determines whether a fracture acts as a conduit or prevents fluid flow. |
| Displacement | The displacement of fracture walls against each other |
| Wall-rock rheology | The uniaxial compressive strength (UCS) and the joint roughness coefficient (JRC) influence fracture closure under increased loading. Furthermore, JRC also controls hydraulic fracture aperture. |
| Aperture | |
| Mechanical ($a_m$) | Real distance between the two walls of a fracture |
| Hydraulic ($a_h$) | Effective hydraulic fracture aperture according to the cubic law |
| Size | |
| Length | The length of the fracture trace on a sampling plane (m) |
| Area | The area of the fracture plane ($m^2$) |
| Volume | The volume of the fracture void ($m^3$) |

size distributions (Priest, 2004), as well as their spatial distribution (Riley, 2005). However, the use of such assumptions may also influence the results. Thus, it is important to systematically quantify the influence of censored fractures to assess the uncertainty of the measured fracture network parameters.

The required number of length measurements and the influence of censored fractures are evaluated in this article by applying the three sampling methods to artificially generated fracture networks with known input parameters. Fracture lengths of natural fracture networks have been reported to follow power-law (e.g., Bonnet et al., 2001), log-normal (Priest and Hudson, 1981), gamma (Davy, 1993), and exponential distributions (Cruden, 1977). However, power-law relationships are the most commonly used to describe the distribution of fracture lengths (e.g., Pickering et al., 1995; Odling, 1997; Blum et al., 2005; Tóth, 2010; LeGarzic et al., 2011). The arguments in favor of power laws are comprehensively discussed by Bonnet et al. (2001). A point in favor of using power-law distributions is the absence of a characteristic length scale in the fracture growth process. However, all power-law distributions in nature are bound by a lower and upper cutoff. The size of a fracture can be restricted, for example, by lithologic layering. The presence of such a characteristic length scale can give rise to log-normal distributions (Odling et al., 1999; Bonnet et al., 2001), although the underlying fracturing is a power-law process. Considering the above, we chose to use a power law to describe the distribution of fracture lengths in this study.

The objective of this study is to further investigate the use and applicability of different sampling methods for the characterization of fracture networks at outcrops. We specifically provide a critical review of the application and limitations for the scanline sampling, window sampling, and circular estimator methods and describe their typical application using two natural fracture networks: (1) lineaments from a satellite image of the Oman Mountains, Oman (Holland et al., 2009a), and (2) fractures from an outcrop at the Craghouse Park, United Kingdom (Nirex, 1997a). In the second part of this study, AFNs are used to evaluate (1) the required minimum number of measurements and (2) the uncertainty of the results for increasing percentages of censored fractures. The results of these analyses are then used to reevaluate the natural examples, to determine which sampling method is best suited, and to provide the uncertainty caused by censoring bias. For the evaluation of the fracture networks, a novel software, called Fracture Network Evaluation Program (FraNEP), was developed.

## FRACTURE SAMPLING AT OUTCROPS

This section provides an overview of (1) typical fracture (Table 1) and fracture network parameters (Table 2), (2) biases related to fracture sampling,

**Table 2.** Definition of Fracture Density ($p$), Intensity ($I$), Spacing ($S$), and Mean Length ($l_m$), and Governing Equations to Calculate These Parameters Using the Scanline Sampling, Window Sampling, and Circular Estimator Methods*

| Parameter | | Definition | Scanline Sampling** | Window Sampling** | Circular Estimator** |
|---|---|---|---|---|---|
| Density ($p$) | Areal (P20) | Number of fractures per unit area ($m^{-2}$) | – | $p_{WS} = \frac{N}{A}$ | $p_{CE} = \frac{m}{2\pi r^2}$ |
| | Volumetric (P30) | Number of fractures per unit volume ($m^{-3}$) | – | – | – |
| Intensity ($I$) | Linear (P10) | Number of fractures per unit length ($m^{-1}$) | $I_{SLS} = \frac{N}{L}$ | – | – |
| | Areal (P21) | Fracture length per unit area ($m \times m^{-2}$) | – | $I_{WS} = \frac{\sum l}{A}$ | $I_{CE} = \frac{n}{4r}$ |
| | Volumetric (P32) | Fracture area per unit volume ($m^2 \times m^{-3}$) | – | – | – |
| Spacing ($S$) | Linear | Spacing between fractures (m) | $S = \frac{1}{I_{SLS}}$ | – | – |
| Mean length ($l_m$) | Linear | Mean fracture length (m) | $l_{m;SLS} = \frac{\sum l}{N}$ | $l_{m;WS} = \frac{\sum l}{N}$ | $l_{m;CE} = \frac{\pi r}{2} \frac{n}{m}$ |
| Length distribution | 1-D** | Fractures intersecting with a scanline | Yes | – | – |
| | 2-D** | Fractures intersecting with a sampling area | – | Yes | – |
| Orientation | 2-D** | Orientation of a fracture on a sampling plane | Yes | Yes | – |
| | 3-D** | Orientation of a fracture in a sampling volume | (Yes)†,†† | (Yes)†† | – |

*The latter is based on Rohrbaugh et al. (2002). The definitions of fracture length distributions and orientations evaluated by the scanline sampling and window methods are also included. Dershowitz (1984) introduced notations to distinguish between linear, areal, and volumetric fracture densities and intensities (P20, P30, etc.)

**$N$ = the total number of sampled fractures; $L$ = the scanline length; $A$ = the sampling area; $r$ = the radius of the circular scanline; $l$ = the fracture length; $n$ and $m$ = the number of intersections with a circular scanline and the number of endpoints in a circular window enclosed by the circular scanline, respectively. The subscripts *WS* (window sampling), *SLS* (scanline sampling), and *CE* (circular estimator) of the parameters indicate the corresponding sampling method. 1-D = one-dimensional; 2-D = two-dimensional; 3-D = three-dimensional.

†Borehole: possible for oriented well cores and image logs.

††Outcrop: possible for three-dimensional outcrop settings.

and (3) the application of the three typical sampling methods used for outcrop analysis. The methods presented are the scanline sampling, window sampling, and circular estimator methods (Figure 1). In addition, we summarize typical techniques to correct the sampling biases associated with these methods. Finally, previous comparisons of sampling methods are presented.

## Fracture and Fracture Network Parameters

Based on geometric data, statistical distributions, and relationships between fracture network parameters, AFNs can be generated stochastically to predict the fluid-flow behavior in fractured reservoirs under different scenarios (Berkowitz, 2002; Castaing et al., 2002; Neuman, 2005; Toublanc et al., 2005; Blum et al., 2009). Typical parameters for AFN characterization are fracture density, intensity, spacing, mean length or length distribution, and orientation of fractures (Priest, 1993; Narr, 1996; Mauldon et al., 2001; Castaing et al., 2002; Ortega et al., 2006; Blum et al., 2007; Neuman, 2008).

Fracture length and length distribution are important parameters for flow simulations. However, the definition of fracture lengths at outcrops is a challenging task. For example, fractures identified as single strands at one scale of observation (e.g., satellite image) may be seen as linked segments when changing the scale of observation (e.g., at ground level). Moreover, the intersection of different fractures (e.g., Ortega and Marrett, 2000) and fracture cementation (e.g., Olson et al., 2009; Bons et al., 2012) add significant complexity to the identification of individual fractures. Simulating fluid transport in an AFN generated from well-characterized but irrelevant fractures will provide irrelevant results. Hence, it is important to link the observations in the subsurface with those obtained at outcrops. This can be accomplished by a comparison of scanline measurements (e.g., fracture apertures) from well cores or image logs with those from outcropping subsurface analogs.

Mean fracture length is another commonly used parameter. Here, we want to briefly address the

issue of evaluating a mean length for a power-law distribution of fracture lengths. Considering the absence of a characteristic scale of power laws and the limited information on lower and upper cutoff lengths for natural systems, a mean value is only valid for the sampled fracture length population. Using such a parameter, for example, for fluid-flow upscaling is therefore meaningless.

Additional information is necessary to quantify fluid flow through fracture networks, including fracture filling, displacement, wall rock rheology, and mechanic or hydraulic fracture aperture (e.g., Lee and Farmer, 1993; Barton and de Quadros, 1997; Odling et al., 1999; Renshaw et al., 2000; Laubach, 2003; Laubach and Ward, 2006; Llewellin, 2010). For a better prediction of fractures in diagenetically and structurally complex settings, evidence of the loading and mechanical property history of the host rock, as well as current mechanical states, are also required (Laubach et al., 2009). A summary of fracture (Table 1) and fracture network parameters (Table 2) is provided below.

## Sampling Biases and Correction Techniques

Orientation, truncation, censoring, and size bias, among others, can cause significant under- or overestimation of statistical parameters and can thus potentially prejudice the characterization of fracture networks (Zhang and Einstein, 1998).

Orientation bias is caused by fractures that intersect the outcrop surface or scanline at oblique angles. Thus, an apparent distance, or spacing, is measured between two adjacent fractures, which cause an underestimation of fracture frequency (Figure 1A). A typical correction method for orientation bias is the Terzaghi correction (Terzaghi, 1965; Priest, 1993), where the apparent distance ($S_A$) is corrected by the cosine of the acute angle $\theta$ of the fracture normal and the scanline or scan surface to obtain the true spacing ($S$):

$$S = S_A \times \cos\theta \qquad (1)$$

Linear fracture intensity, which is also commonly referred to as fracture frequency, is equal to $1/S$. In three dimensions, $\cos\theta$ is given by (Hudson and Priest, 1983):

$$\cos\theta_i = \cos(\alpha - \alpha_i)\cos\beta\cos\beta_i + \sin\beta\sin\beta_i \qquad (2)$$

where $\alpha$ and $\beta$ are the dip direction and dip of the scanline, and $\alpha_i$ and $\beta_i$ are the dip direction and dip of the $i$th fracture set normal. The problem with this correction method is that fractures have to be grouped into fracture sets. An alternative technique is presented by Lacazette (1991), which corrects the orientation bias for each individual fracture:

$$\text{Occurence} = \frac{1}{L \times \cos\theta} \qquad (3)$$

where occurrence may be thought of as the frequency of an individual fracture, $L$ is the length of a scanline, and $\alpha$ is the angle between the pole to the fracture and the scanline. The fracture frequency of a set is the sum of the occurrence parameters calculated for the individual fractures in this set. A method presented by Narr (1996) allows estimating the average fracture spacing in the subsurface. The method uses the spacing and height of fractures and the borehole diameter to predict fracture intersection frequencies for all possible well deviations.

Truncation bias is caused by unavoidable resolution limitations, which depend on the used detection device (e.g., satellite image, human eye, or microscope) and the contrast between the host rock and fractures. Parameters such as fracture size (length or width) are not detectable below a certain scale. Moreover, as fracture size approaches the detection limit, the actual number of recognized fractures significantly decreases. Thus, defining a lower cutoff of fracture size based on data resolution is needed to correct truncation bias (Nirex, 1997b). The truncation bias of sampled fracture lengths can be corrected by applying the chord method (Figure 1B) (Pérez-Claros et al., 2002; Roy et al., 2007). Bonnet et al. (2001) plotted lower cutoff lengths against sampling areas reported in literature and could show that the cutoff lengths are typically in the range of 0.5% to 25% of the square root of the sampling area, with an average of approximately 5%.

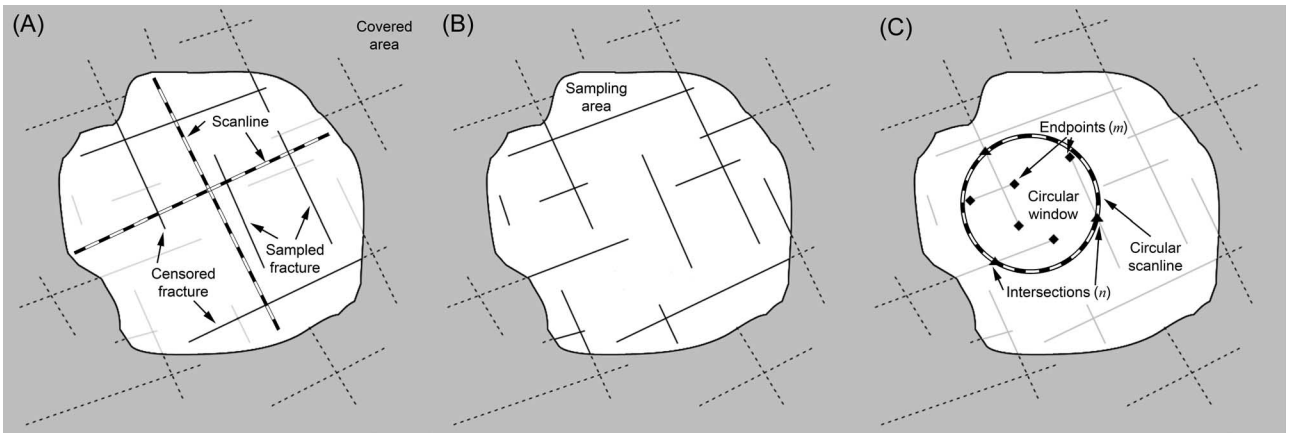


**Figure 2.** Window sampling (A), scanline sampling (B), and circular estimator method (C). Solid black lines indicate sampled fractures; light gray lines, nonsampled fractures; and dashed lines, the nonobservable (censored) parts of fractures (modified from Rohrbaugh et al., 2002).

Censoring bias is typically related to a limited outcrop size (Type I: fractures with one or both ends outside the sampling area), uneven outcrops (e.g., erosion features), and coverage by overlaying rock layers or vegetation (Type II: fractures with both ends inside the sampling area but partly hidden from observation) (Figure 1C) (Priest, 1993; Pickering et al., 1995; Zhang and Einstein, 2000; Bonnet et al., 2001; Rohrbaugh et al., 2002; Fouché and Diebolt, 2004). The focus of this study is on Type I. A typical effect of this censoring bias is an overestimation of fracture density (Kulatilake and Wu, 1984; Mauldon et al., 2001). For this type of censored fractures, it is impossible to know the relative lengths of the visible and censored parts. Therefore, it is also impossible to tell whether the fracture center is inside the sampling area or not. However, it can be assumed that half of these fracture centers should be inside, and the other half, outside the sampled area. Thus, half of the censored fractures can be neglected for the calculation of fracture density (Mauldon, 1998; Mauldon et al., 2001; Rohrbaugh et al., 2002). For Type II censored fractures, we know that the center is inside the sampling area. Unfortunately, if a fracture transects a covered part of the outcrop, it is impossible to tell whether we look at one transecting fracture or two fractures with obscured ends. To make a prediction whether we look at a transecting fracture or not, the true fracture length distribution needs to be known. However, correcting censoring bias for fracture length distributions is complex, and a complete review is beyond the scope of this study. Detailed descriptions on this topic are provided by, for example, Priest (2004) and Riley (2005).

Size bias is associated with the scanline sampling method (Bonnet et al., 2001; Manzocchi et al., 2009). Because the probability of a fracture to intersect a scanline is proportional to its length, shorter fractures are underrepresented in the measurements gathered along scanlines (Figure 2A) (Priest, 1993; LaPointe, 2002). Possible correction techniques are provided below, along with the description of the scanline sampling method.

## Scanline Sampling

The scanline sampling method (Figure 2A, Table 2) is based on data collection from all fractures that intersect a scanline (Priest and Hudson, 1981; Priest, 1993; Bons et al., 2004). The method allows a quick measurement of fracture characteristics in the field and is the main method used for the analysis of borehole image logs and cores. Its application provides one-dimensional (1-D) information on fracture networks (Table 2). The method is affected by (1) orientation bias, (2) truncation bias, (3) censoring bias, and (4) size bias. Orientation bias can be reduced or even avoided by placing a scanline perpendicular to a fracture set. If necessary, several scanlines can be used in outcrops to capture different fracture sets. However, well logs and drill cores constitute only one single scanline.

Several additional equations and assumptions are necessary to (1) correct size bias, (2) compare linear with areal fracture intensity (Table 2), and (3) evaluate fracture density. The assumptions and equations provided here are only valid for power-law distributions of fracture lengths and need to be modified for other distributions. If we assume uniformly distributed, disc-shaped fractures with a power-law distribution of disc diameters in three dimensions, the fracture lengths measured in a plane also follow a power law. The relationship between three-dimensional (3-D), two-dimensional (2-D), and 1-D exponents of a power-law length distribution follows (Darcel et al., 2003):

$$E_{3\text{-}D} = E_{2\text{-}D} + 1 = E_{1\text{-}D} + 2 \tag{4}$$

where $E_{3\text{-D}}$ is the exponent for a 3-D rock mass volume, $E_{2\text{-D}}$ is the exponent for a 2-D sampling area, and $E_{1\text{-D}}$ is the exponent for a 1-D scanline. However, fractures in stratified rocks are probably not disc shape. Moreover, equation 4 is only valid for well-sampled representative populations of uniformly distributed fractures. For fractures with strong spatial correlation, clustering, or directional anisotropy, Hatton et al. (1993) provide a more appropriate relationship between 3-D and 2-D exponents:

$$E_{3\text{-}D} = A \times E_{2\text{-}D} + B \tag{5}$$

where $A = 1.28 \pm 0.30$ and $B = -0.23 \pm 0.36$. Because it is impossible to evaluate 2-D exponents from scanline measurements using equation 5, we use equation 4.

Size bias causes an overestimation of mean fracture length. For a given minimum fracture length $l_0$, a mean length $l_m$ can be calculated as follows (LaPointe, 2002):

$$l_m = \frac{E_{2\text{-}D} l_0}{E_{2\text{-}D} - 1} = \frac{(E_{1\text{-}D} + 1) l_0}{E_{1\text{-}D}} \tag{6}$$

The scanline sampling method estimates linear fracture intensity $P10$ (Table 2), which is commonly also referred to as frequency. A relationship between linear ($P10$) and volumetric ($P32$) fracture intensities (Table 2) is provided by Barthélémy et al. (2009):

$$P10 = P32 \times e[\cos(\theta)] \tag{7}$$

where $e[cos(\theta)]$ is the expected mean of the cosines of angles $\theta$ for the fractures of one set. For a scanline parallel to the normal of a fracture set, $e[cos(\theta)]$ equals 1, thus the relationship between linear ($P10$), areal ($P21$), and volumetric ($P32$) fracture intensities (Table 2) is given by

$$P10 = P21 = P32 \tag{8}$$

Fracture intensity $I$ is defined as the product of density $p$ and mean length $l_m$:

$$I = p \times l_m \tag{9}$$

The combination and rearrangement of equations 4, 8, and 9 allow estimating areal fracture density based on measurements obtained by the scanline sampling method:

$$p = \frac{P10}{l_m} = \frac{P10 \times E_{1\text{-}D}}{(E_{1\text{-}D} + 1) \times l_0} \tag{10}$$

## Window Sampling

The window sampling method (Figure 2B; Table 2) estimates the statistical properties of fracture networks by measuring parameters from all fractures present within the selected sampling area (Pahl, 1981; Wu and Pollard, 1995). Typical applications of this method are the analysis of outcropping subsurface analogs (Belayneh et al., 2009) or the characterization of fracture networks using remote sensing data from satellite images or aerial photographs (Koike et al., 1995; Becker, 2006; Holland et al., 2009a; Zeeb et al., 2010). In general, three types of sampling bias affect the window sampling method: (1) orientation, (2) truncation, and (3) censoring biases.

### Circular Estimator

The circular estimator method uses a combination of circular scanlines and windows (Mauldon et al.,

2001; Figure 2C). It is in fact a maximum likelihood estimator (Lyman, 2003). This means that, instead of directly sampling individual fractures and measuring their characteristics, for example, orientation or length, parameters are estimated using statistical models that are described in detail by Mauldon et al. (2001). Based on the number of intersections ($n$) between a circular scanline and fractures and the number of fracture endpoints ($m$) in a circular window formed by this scanline, fracture density, intensity, and mean length are calculated (Table 2). To assure an accuracy of the results of 15% or higher, ten circular scanlines with a diameter exceeding the mean fracture block size, or fracture spacing, but significantly smaller than the minimum dimension of the sample region, are randomly placed in the sampling area (Rohrbaugh et al., 2002). In addition, $m$ counts should be higher than 30 (Rohrbaugh et al., 2002). The circular estimator is a time-efficient method to evaluate fracture network characteristics. Being a maximum likelihood estimator, the method is not subject to sampling bias. However, this method does not provide information on important parameters such as fracture orientation, length distribution, or width. Hence, it should, in principle, be combined with other sampling methods.

### Comparison of Different Sampling Methods in the Literature

Several studies compared the effectiveness of the different sampling methods for specific case studies. For example, Belayneh et al. (2009) conducted water-flooding numerical simulations on deterministic and stochastic discrete fracture networks and matrix models. To generate these networks, outcropping subsurface analogs of Jurassic carbonate platforms on the southern margin of the Bristol Channel Basin were studied using the window sampling and scanline sampling methods. The measured parameters included fracture orientation, length, spacing, and aperture. Numerical simulations on deterministic models (window sampling) showed that flow is fracture-dominated. Simulating flow through fracture network models (scanline sampling) varied from fracture to matrix dominated. They concluded that this uncertainty may be caused by the undersampling of fractures along scanlines. Manda and Mabee (2010) studied the effectiveness of the single scanline, the multiple scanline, and the window sampling methods, using them to acquire the properties of fractures from layered dolomites in a quarry in Wisconsin. They used overall volumetric intensity and permeability of fracture network models to assess the accuracy of these methods and recommended the use of the window sampling method. Weiss (2008) used the scanline sampling, window sampling, and circular estimator methods to characterize fracture networks from chalk in the northern Negev in Israel. He concluded that the circular estimator method is a useful tool to assess mean fracture size without the need of accounting for sampling bias. However, the sampling areas were very limited in size. Hence, large fractures controlling the fluid transport in the aquifer were not adequately defined by the relatively small circular and rectangular sampling windows. Weiss (2008) suggested a combination of the scanline and window sampling methods to calculate the distribution of fracture length. Rohrbaugh et al. (2002) used AFNs with scale-dependent length distributions to investigate the accuracy of the results from the scanline sampling, window sampling, and circular estimator methods in estimating fracture density, intensity, and mean length. Based on their results, Rohrbaugh et al. (2002) presented a guideline for the application of the circular estimator method and followed this guideline to characterize eight natural fracture networks.

## STUDY OF NATURAL FRACTURE NETWORKS

In this section, we show a typical application of the scanline sampling, window sampling, and circular estimator methods. The fracture network parameters of two natural examples are evaluated: (1) lineaments measured from a satellite image of the Oman Mountains, Oman (Figure 3; from Holland et al., 2009a) and (2) fractures from an outcrop located at Craghouse Park, United Kingdom (Figure 4; Nirex 1997a, b). The three sampling

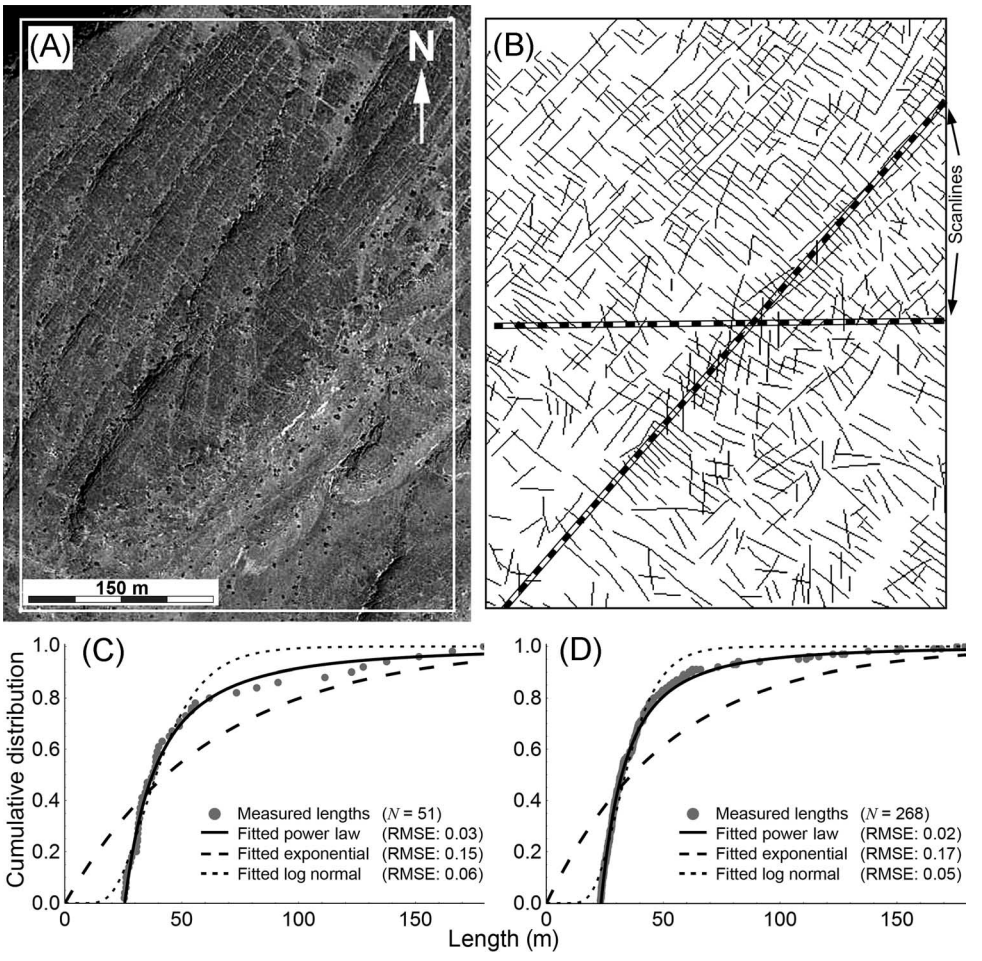


**Figure 3.** (A) Satellite image from the southern flank of the Jabal Akhdar dome in the Oman Mountains, Oman (enhanced satellite image from Google, GeoEye [Digital Globe]). (B) Interpretation of the fractures in the white rectangle in panel A after the correction of truncation bias (modified from Holland et al., 2009a). The UMT coordinates on the lower left and upper right corners are 40N 525496 2562373 and 40N 525799 2562760, respectively. Please note that the satellite image and the trace line map are not to scale because of the slope of the flank. Panels C and D show a plot of fracture lengths (gray dots) against the cumulative distribution measured by two scanlines (C) and one window sampling (D) of the whole study area (A). The solid, dashed, and dotted black lines indicate power-law, exponential, and log-normal fits. The fitting accuracy is given by root-mean-square errors (RMSE).

methods are used to estimate fracture density, intensity, mean length, and length distribution.

The first natural fracture network (Figure 3) is an analysis of lineament data (fractures, faults, joints, veins, etc.) extracted from a Quickbird satellite image from the southern flank of the Jabal Akhdar dome in the Oman Mountains, Oman (Hilgers et al., 2006; Holland et al., 2009a, b). The sampling area has an extent of 120,000 $m^2$ (1,291,669 $ft^2$), in which 650 lineaments with lengths ranging between 3 and 179 m (10 and 587 ft) could be identified by optical picking. Applying the chord method (Pérez-Claros et al., 2002; Roy et al., 2007), the cutoff length for truncation bias is 23.3 m (76.4 ft). For interpretation, the panchromatic band, which offers a spatial resolution of 0.7 m (2.3 ft), was used. Based on the number of fractures extending beyond the boundaries of the sampling area, approximately 5% of the sampled fractures appear to be censored.

The second natural fracture network is an outcrop located at Craghouse Park, United Kingdom (Figure 4; Nirex, 1997a). This sampling area has a size of 19 $m^2$ (205 $ft^2$), containing a total of 288 visible fractures with lengths ranging between 0.05 and 4.0 m (0.16 and 13.1 ft). The application of the chord method (Pérez-Claros et al., 2002; Roy et al., 2007) provided a cutoff length for truncation bias of 0.8 m (2.6 ft). The limited outcrop size, which is typical for a humid climate, causes 30% of the fractures to be censored.

Table 3 summarizes the fracture network parameters obtained from the two natural examples. The deviation between the results for length distribution exponents evaluated by scanline and window sampling for the Oman example might be caused by difficulties when interpreting fracture lengths in the satellite image. Erosion features (Figure 3A) cause a type II censoring bias (Figure 1C). Thus, the interpretation of two short fractures is actually one long

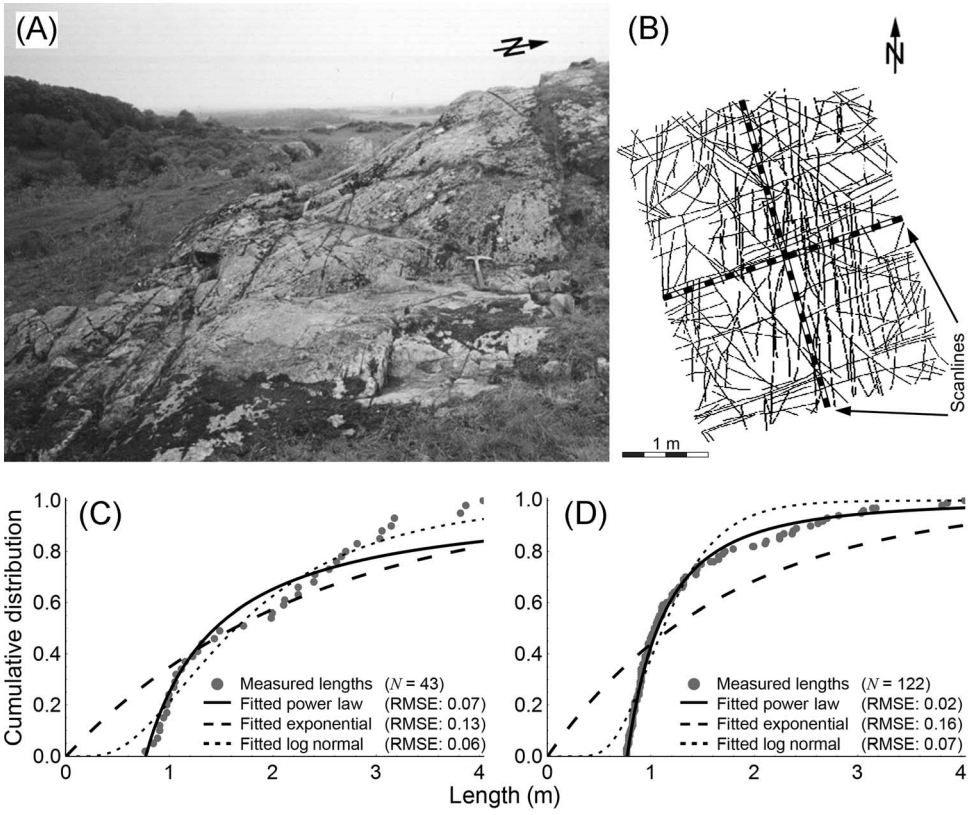


**Figure 4.** (A) Photograph of the investigated outcrop at Craghouse Park, United Kingdom (geologic hammer for scale). (B) Trace line map of the cleaned outcrop. Panels C and D show a plot of fracture lengths (gray dots) against the cumulative distribution measured by two scanlines (C) and one window sampling (D) of the whole study area (A). The fitting accuracy is given by the root-mean-square error (RMSE).

fracture. Moreover, what looks like one long fracture in the satellite image might be a series of fracture segments when studied at the ground level.

When analyzing the second example from the United Kingdom, a power-law length distribution was assumed. Such an assumption is valid (and necessary), if an upscaling of the results is intended. If the length distribution at the scale of observation is evaluated, then a log-normal distribution is probably a better choice. However, the length measurements should not be corrected for truncation bias because the procedure removes the short fracture lengths, which are essential for a log-normal distribution.

For the analysis of both natural examples, it was impossible to sample 30 fracture endpoints

**Table 3.** The Fracture Network Parameters Estimated for the Two Natural Fracture Networks*

| Location | Oman Mountains (Oman) | | | Craghouse Park (United Kingdom) | | |
|---|---|---|---|---|---|---|
| Parameter | Scanline Sampling | Window Sampling | Circular Estimator | Scanline Sampling | Window Sampling | Circular Estimator |
| Number of measurements | 51 | 268 | – | 43 | 122 | – |
| Length range (m) | 25.6–179 | 23.3–179 | – | 0.8–4.0 | 0.8–4.0 | – |
| Radius (m) | – | – | 100 | – | – | 1.6 |
| Censored fractures (%) | 0 | 5 | – | 11 | 30 | – |
| Density, $p$ ($m^{-2}$) | 0.002 | 0.002 | 0.002 | 3.5 | 5.4 | 2.8 |
| Intensity, $I$ ($m \times m^{-2}$) | 0.07 | 0.09 | 0.10 | 5.1 | 7.4 | 3.6 |
| Mean length, $l_m$ (m) | 39.7 | 41.6 | 53.9 | 1.5 | 1.4 | 1.3 |
| Exponent, $E_{2\text{-}D}$ | 2.8 | 2.2 | – | 2.1 | 2.2 | – |

*The results are corrected for orientation, truncation, and size bias. Half of the type I censored fractures (Figure 1) were neglected when calculating fracture density applying the window sampling method.

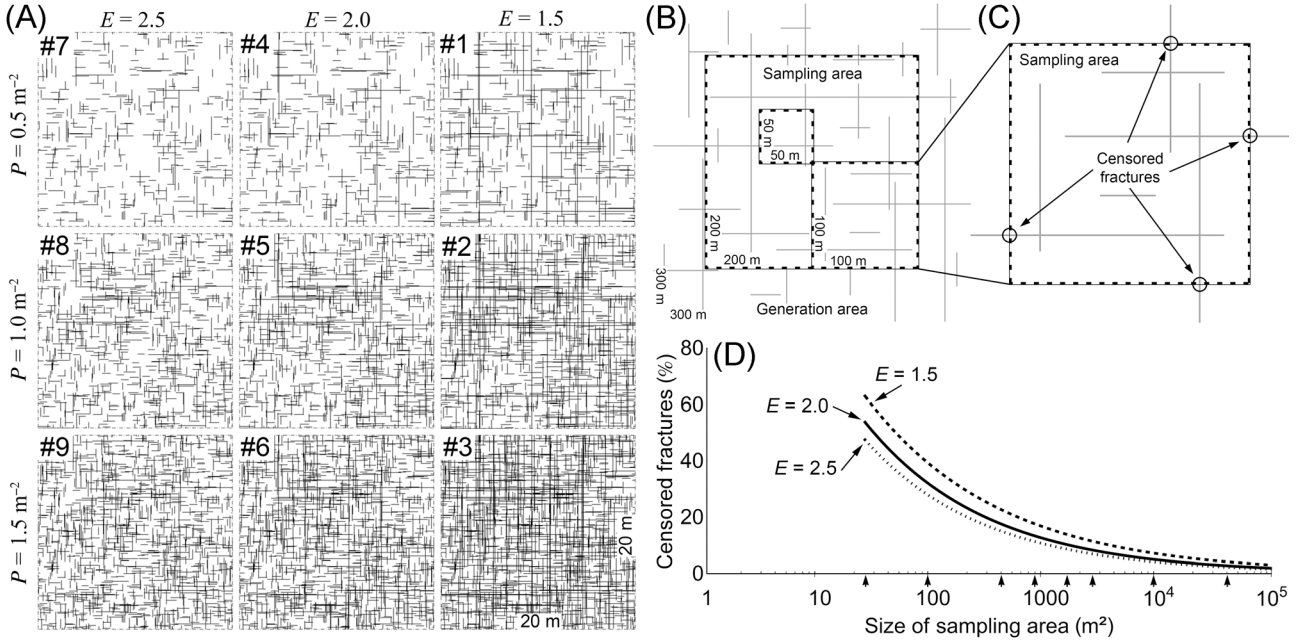


**Figure 5.** (A) Examples for a 20 × 20 m (66 × 66 ft) sampling area from each of the nine two-dimensional artificial fracture networks, with input values for fracture density in number per square meter ($p$) and exponent ($E$) of the power-law length distribution. The numbering of the artificial fracture network corresponds to those in Table 4. (B) Sketch illustrating the generation area and the definition of sampling areas. (C) Definition of the censored fractures in a sampling area. (D) The relationship between the size of the sampling area and the average percentage of censored fractures for the three power-law length distributions. The black arrows on the $x$ axis indicate the size of the sampling areas analyzed in this study.

with a radius of the circular scanlines equal to one-tenth of the sampling area extent. Therefore, the radii were increased (Table 3) to satisfy the 30-endpoint criteria defined by Rohrbaugh et al. (2002).

## ARTIFICIAL FRACTURE NETWORKS

In this section, we apply the scanline sampling, window sampling, and circular estimator methods to AFN with known input values and compare them with the calculated fracture network parameters. With this systematic approach we evaluate, for each sampling method, (1) the minimum number of required measurements and (2) the influence of censored fractures on estimates of fracture network parameters.

### Fracture Network Generation

The fracture network generator FracFrac (Blum et al., 2005), a program based on Visual Basic for Applications in Microsoft Excel, was used to generate nine 2-D AFNs (Figure 5). The networks are defined by fracture density and length distribution. For the density, three values with $p = 0.5\ \mathrm{m}^{-2}$ ($0.046\ \mathrm{ft}^{-2}$), $p = 1.0\ \mathrm{m}^{-2}$ ($0.093\ \mathrm{ft}^{-2}$), and $p = 1.5\ \mathrm{m}^{-2}$ ($0.139\ \mathrm{ft}^{-2}$) were assumed. Power-law exponents reported for natural fracture systems typically range between 0.8 and 3.5, with most in the range between 1.7 and 2.8 and most of which are actually approximately 2 (Bonnet et al., 2001). For the generation of the AFN, we used exponents of $E$ = 1.5, $E$ = 2.0, and $E$ = 2.5. In this study, a truncated power law is used to describe the cumulative distribution of fracture lengths (Blum et al., 2005; Riley, 2005):

$$f(l) = 1 - \left(\frac{l}{l_0}\right)^{-E} \qquad (11)$$

We define a lower cutoff length $l_0$ of 1 m (3 ft). Although Odling et al. (1999) observed a similar cutoff for joints in sandstones of western Norway,

**Table 4.** Summary of the True Fracture Network Parameters for the Nine Generated Artificial Fracture Networks*

| | Artificial Fracture Network | | | | | | | | |
|---|---|---|---|---|---|---|---|---|---|
| Parameter | 1 | 2 | 3 | 4 | 5 | 6 | 7 | 8 | 9 |
| Density, $p$ ($m^{-2}$) | 0.5 | 1.0 | 1.5 | 0.5 | 1.0 | 1.5 | 0.5 | 1.0 | 1.5 |
| Intensity, $I$ ($m \times m^{-2}$) | 1.5 | 3.0 | 4.5 | 1.0 | 2.0 | 3.0 | 0.8 | 1.7 | 2.5 |
| Mean length, $l_m$ (m) | 3.0 | 3.0 | 3.0 | 2.0 | 2.0 | 2.0 | 1.7 | 1.7 | 1.7 |
| Exponent, $E_{2\text{-}D}$ | 1.5 | 1.5 | 1.5 | 2.0 | 2.0 | 2.0 | 2.5 | 2.5 | 2.5 |

*Values for fracture intensity and mean length are calculated from the fracture density and power-law exponent used as input by applying equations 4 and 7.

this value is probably only valid for this specific case study. The lower cutoff is necessary to constrain the range of fracture lengths in the AFNs and is an arbitrary value.

Table 4 provides a summary of true fracture density, intensity, mean length, and power-law exponent for each of the nine AFNs (Figure 5A). Orientation bias is avoided using two sets of perfectly parallel fractures with orientations of 90° and 180°. Furthermore, the input fracture density is equally distributed between the two fracture sets.

The generation area of each AFN is 300 × 300 m (984 × 984 ft). In this whole area, a total of 146 squared sampling areas are defined (one area with an edge length of 200 m [656 ft]; four with 100 m [328 ft]; 16 with 50 m [164 ft]; and 25 sampling areas with edge lengths of 40 m [131 ft], 30 m [98 ft], 20 m [66 ft], 10 m [33 ft], and 5 m [16 ft]), providing a total of 1314 sampling areas for all nine AFNs (Figure 5B). Fractures are treated as censored, if one or both ends intersect with a boundary of the sampling area (Figure 5C). The percentage of censored fractures is calculated from the total number of fractures in a sampling area and the number of fractures that are censored. Figure 5D presents the percentages of censored fractures averaged for the different sized sampling areas. The highest percentages are found for small sampling areas and high power-law exponents (Figure 5A; $E = 1.5$).

Each sampling area is analyzed using FraNEP. FraNEP is a novel software that characterizes fracture networks applying either the scanline sampling, window sampling, or circular estimator methods. For the scanline sampling method, one scanline is placed perpendicular to each of the two fracture sets. The window sampling method is applied on the entire sampling area. For the application of the circular estimator method, we follow the guideline of Rohrbaugh et al. (2002). Ten circular scanlines are randomly placed inside the sampling area, with the radius equal to one-tenth of the edge length. Values for fracture density, intensity, mean length, and length distribution are calculated and compared with the true values. For the calculation of the fracture density, half of the censored fractures are neglected. For the other three parameters, all sampled fractures are used. The distribution of fracture lengths is evaluated by fitting power-law, log-normal, and exponential cumulative distribution functions to the sampled fracture lengths. The root-mean-square error approach is used to compare the quality of a best fit, which is calculated from the sum of squared errors, the number of measurements, and the mean value of the measured parameter (Loague and Green, 1991).

Table 5 provides an example for three sizes of sampling areas from AFN 5. Shown are the range of values (lowest to highest) of calculated fracture network parameters for all sampling areas of the same size. Table 5 illustrates well how the spread of values, and thus the uncertainty, increases for smaller sampling areas. For fractures sampled by scanline sampling in the 10 × 10 m (33 × 33 ft) sampling area, fracture lengths follow a log-normal distribution. We conclude that scanline sampling does not suffice to characterize these sampling areas. Figure 6 shows fracture lengths and fitted distributions for one exemplary sampling area from each size presented in Table 5. The fitting accuracy of the power-law distribution decreases for smaller sampling areas.

**Table 5.** Examples of Fracture Network Parameters Evaluated for Artificial Fracture Network 5*

| Edge Length (m) | Sampling Method** | Value Range: Density ($1\ m^{-1}$) ($p$ = 1.0) | Intensity ($m \times m^{-2}$) ($I$ = 2.0) | Mean Length (m) ($l_m$ = 2.0) | Exponent ($E_{2\text{-}D}$ = 2.0) |
|---|---|---|---|---|---|
| | SLS | 0.96–1.08 | 1.87–2.16 | 1.92–2.05 | 1.95–2.09 (4/4)† |
| 100 | WS | 0.99–1.00 | 1.96–2.01 | 1.93–1.98 | 1.97–2.02 (4/4)† |
| | CE | 0.94–1.00 | 1.82–2.20 | 1.93–2.21 | – (4/4)†† |
| | SLS | 0.74–1.21 | 1.50–2.40 | 1.77–2.19 | 1.84–2.27 (25/25)† |
| 40 | WS | 0.96–1.04 | 1.87–2.08 | 1.80–1.97 | 1.90–2.11 (25/25)† |
| | CE | 0.90–1.07 | 1.88–2.63 | 2.03–2.58 | – (25/25)†† |
| | SLS | 0.35–1.30 | 1.00–2.80 | 1.49–4.27 | 1.99–3.03 (2/25)† |
| 10 | WS | 0.83–1.16 | 1.45–2.64 | 1.35–1.97 | 1.54–2.62 (25/25)† |
| | CE | – | – | – | – (0/25)†† |

*Shown are the lowest and highest value found by the three sampling methods in all sampling areas of the presented sizes. The numbers in brackets are the input values.
**SLS = scanline sampling; WS = window sampling; CE = circular estimation.
†Number of sampling areas with power-law distribution of fracture lengths/sampling areas.
††Number of sampling areas with $m$ counts greater than 30/sampling areas.

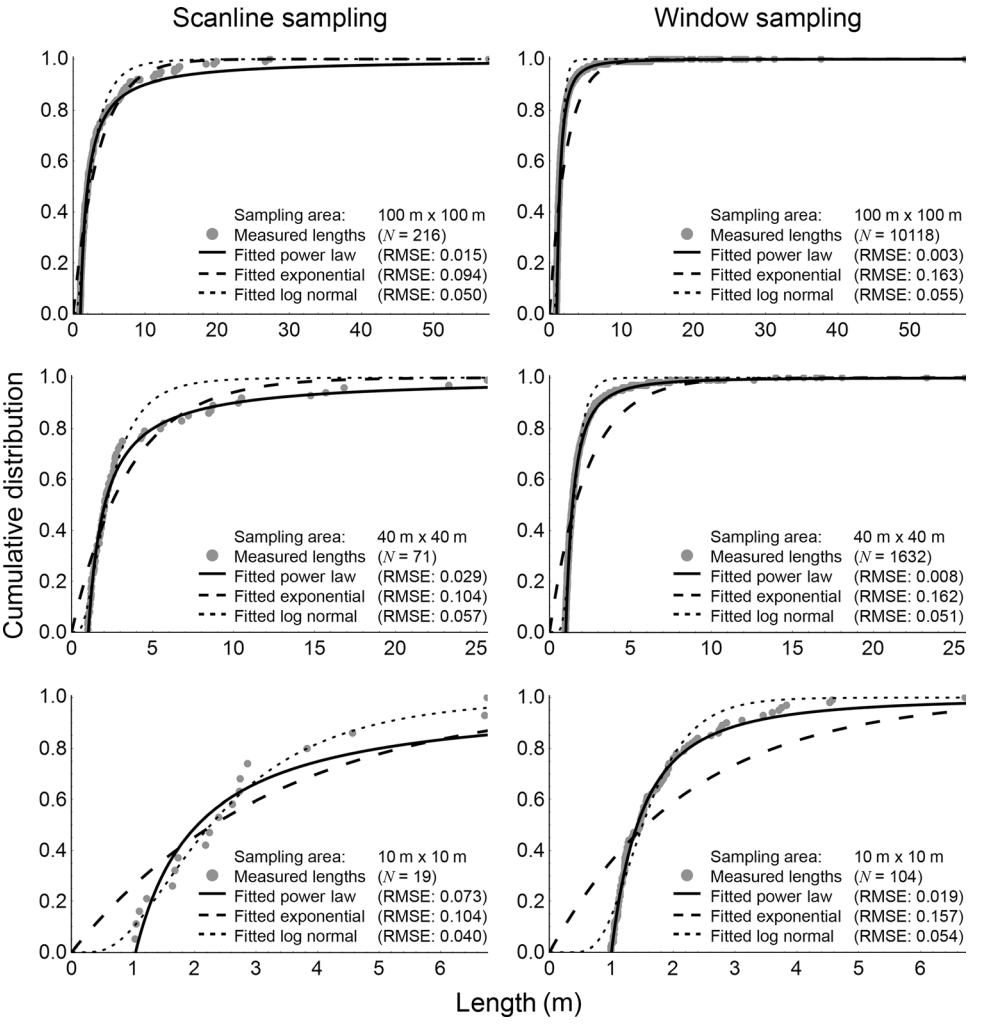


**Figure 6.** Plot of measured fracture lengths (gray dots) against their cumulative distribution. The root-mean-square error (RMSE) in the brackets indicates the accuracy of the fits.

**Table 6.** The Required Minimum Number of Measurements for Each Sampling Method (Value is Underlined)*

| | Number of Measurements | | | | | |
|---|---|---|---|---|---|---|
| Sampling Method | Window Sampling** | | Scanline Sampling** | | Circular Estimator† | |
| 1 | 78 | 83 | 88 | 123 | 846 | 849 |
| 2 | 46 | 106 | 152 | 165 | 478 | 908 |
| 3 | 64 | 65 | 224 | 225 | 710 | 1364 |
| 4 | 78 | 79 | 48 | 49 | 858 | 860 |
| 5 | 38 | 39 | 106 | 107 | 466 | 919 |
| 6 | 53 | 58 | 58 | 61 | 684 | 686 |
| 7 | 78 | 80 | 46 | 47 | 821 | 823 |
| 8 | 110 | 112 | 91 | 97 | 460 | 875 |
| 9 | 53 | 54 | 48 | 50 | 675 | 1315 |
| Criterion | Not satisfied | Satisfied | Not satisfied | Satisfied | Not satisfied | Satisfied |

*The sampling method numbers correspond to the artificial fracture network numbers in Table 4. The numbers for the nine artificial fracture networks in the columns "not satisfied" are the highest number of measurements for which the criteria "window sampling" and "scanline sampling" were not satisfied. The numbers in the columns "satisfied" are the lowest number of measurements above which the criteria "window sampling" and "scanline sampling" were always satisfied.

**Criterion: power-law fits best the fracture length distribution.

†Criterion: circular window contains more than 30 fracture endpoints.

## Required Minimum Number of Measurements

No well-established criteria exist to define the required minimum number of measurements to sufficiently capture the statistical properties of fracture networks using specific sampling methods. For each sampling method, a criterion is defined in such a way that it sufficiently captures the statistical properties. For the scanline and window sampling methods, we defined the criterion as the number of measurements, above which a power law always provides the best fit to the fracture length measurements (Figure 6). The criterion of the circular estimator method is defined as the number of fractures in a sampling area above a circular window always contains 30 or more fracture endpoints (Rohrbaugh et al., 2002). These criteria are applied to the data obtained by the three sampling methods for each of the 146 sampling areas defined within each of the 9 AFNs. Furthermore, two numbers are evaluated for each sampling method: (1) the highest number of measurements that does not satisfy the criterion in any of the 146 sampling areas (Table 6: not satisfied), and (2) the lowest number of measurements above which the criterion is always satisfied in any of the 146 sampling areas (Table 6: satisfied). This is repeated for all nine AFNs. However, these numbers are fracture network specific and depend on the properties of the network. Thus, for the determination of the minimum number, which is universally applicable to all nine studied AFNs, we need to compare these results. The lowest number of 2, which is also higher than all numbers of 1, is the required minimum number of measurements of the sampling method (Table 6).

At least 112 fractures should be measured for the window sampling method; 225 for the scanline sampling method; and 860 for the circular estimator method. Because only the fractures intersecting with a line are considered for the scanline sampling method, significantly more fractures have to be present in a sampling area to measure 225 fractures. For sampling areas with a simple geometry and fracture network pattern, for example, similar to the AFNs, approximately 4000 fractures should be present. A more complex sampling area or fracture network may imply that even more fractures have to be present. Note that the required minimum corresponds to the number of measurements after accounting for truncation bias. Despite the efforts to universally find a minimum number of measurements to properly capture the properties of fracture networks, each case study may require a different minimum number of measurements depending on the network itself.

**Table 7.** Fracture Network Parameters Evaluated for the Two Natural Fracture Networks*

| Parameter | Oman Mountains (Oman) | | Craghouse Park (United Kingdom) | |
|---|---|---|---|---|
| Number of fractures | 268 | | 122 | |
| Length range (m) | 23.3–179 | | 0.76–4.04 | |
| Censored fractures (%) | 5 | | 30 | |
| Density, $p$ ($m^{-2}$) | 0.002 | (Insignificant) | 5.44 | (4.52–6.80) |
| Intensity, $I$ ($m \times m^{-2}$) | 0.09 | (0.09–0.10) | 7.40 | (<< 3.70 – >> 11.1) |
| Mean length, $l_m$ (m) | 41.6 | (41.6–46.2) | 1.36 | (1.33–1.84) |
| Exponent, $E_{2\text{-}D}$ | 2.15 | (2.06–2.21) | 2.17 | (1.69–2.65) |

*The values in brackets indicate the range of possible true values caused by the uncertainty.

## Uncertainty Analysis

The effects responsible for censoring bias are well known. However, to our knowledge, the actual influence of censored fractures on estimates of fracture network parameters has not been comprehensively investigated. The influence is assessed here for four typical fracture network parameters: (1) fracture density, (2) intensity, (3) mean length, and (4) length distribution. For each sampling area, which contains the necessary minimum number of fractures to apply the respective sampling method, the difference between estimated and input value is calculated. The percentage of censored fractures in this sampling area is plotted against the difference in percentage for each parameter and sampling method. The plots illustrate the maximum difference observed for increasing percentages of censored fractures (Figure 7). In this study the range of potential differences between those maximum differences is referred to as the uncertainty. Figure 7 shows an example for the uncertainty in estimating fracture density using the window sampling method.

Figure 8 summarizes the uncertainty of the four parameters estimated by the three sampling methods. For all sampling methods and parameters, the uncertainty of the measured values clearly increases with the percentage of censored fractures. In general, the results based on the window sampling method indicate the lowest uncertainty, especially for the evaluation of fracture density, mean length, and length distribution. An interesting result is the high uncertainty of all three sampling methods in estimating fracture intensity. Although the circular estimator highly overestimates fracture intensity, the method exhibits the lowest uncertainty. All results obtained by the scanline sampling method are within an 80% confidence interval. However, estimates of fracture density and mean length depend on the correct estimate of a power-law length distribution, and thus, only data sets equal to or above the required minimum number of 225 measurements can be used for the calculations and thus can be conducted for the cases of 0% to 5% censored fractures only.

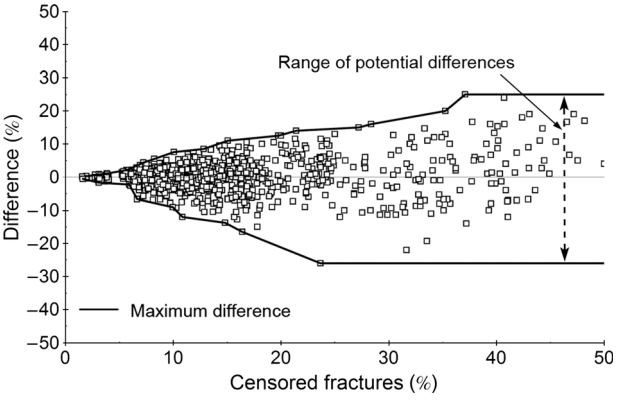


**Figure 7.** Plot of censored fractures (in percent) against the difference (in percent) between estimated and input fracture density for window sampling. Each point represents a sampling area from the nine artificial fracture networks. The maximum difference is highlighted by the two solid black lines. The range of potential differences between those two lines represents the uncertainty of a result for a specific sampling area with the percentage of censored fractures.

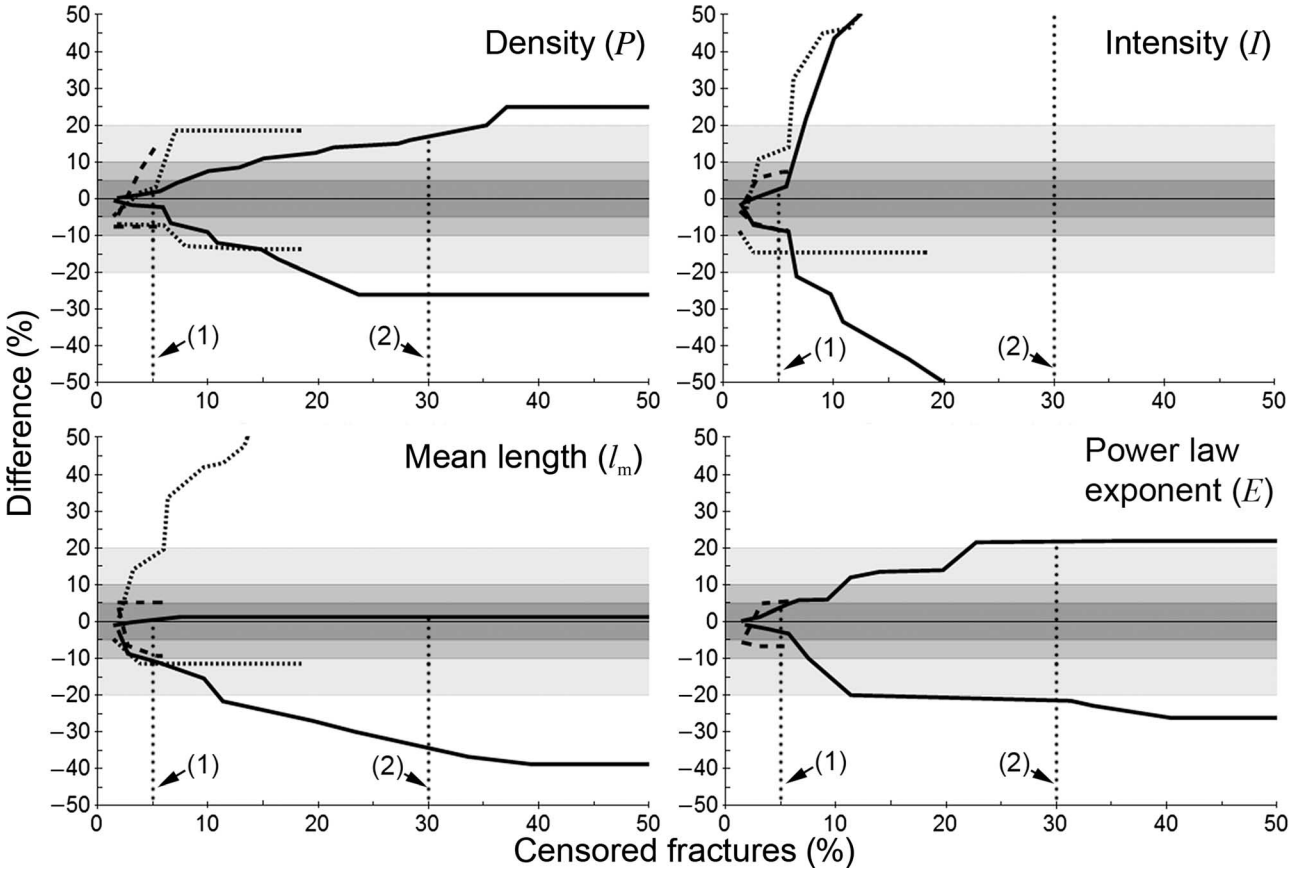


**Figure 8.** Summary of potential differences evaluated for the scanline sampling (dashed), window sampling (solid), and circular estimator (dotted) methods, illustrated as lines of maximum difference (Figure 7). The areas highlighted in dark gray, gray, and light gray represent the 95%, 90%, and 80% confidence intervals of the true value. The vertical dotted lines indicate the percentage of censored fractures for the studied natural fracture networks: the Oman Mountains (1) and the Craghouse Park (2).

## DISCUSSION

Characterizing fracture networks in the subsurface is a challenging task because of the limitations of borehole, borehole log, or core analysis. Studying outcrops analogous to the subsurface provides valuable data, especially on fracture lengths (mean length and length distribution). Additional information on fracture density and intensity can improve our understanding of the subsurface even more. However, the characterization of fracture networks using outcrops is also challenging. The interpretation of a single fracture can change with the scale of observation. For example, a fracture interpreted as a single entity in an aerial photograph can prove to be a segmented fracture at ground level. Moreover, fractures are altered by weathering when exposed; they normally crosscut each other and can be filled, partly or completely, by mineral precipitates or debris. Defining the length, or the endpoints, of a fracture can be difficult under such circumstances. In addition, fracture networks are 3-D, whereas the analysis of boreholes and outcrops are commonly constrained to one or two dimensions, respectively. Therefore, models of subsurface fracture networks can be significantly improved if cross-correlated data from borehole and outcrop analysis are considered.

The main advantage of the scanline sampling and window sampling methods is the comprehensive information on the fracture parameters they provide, especially measurements of fracture length, aperture, and orientation. However, the two methods are subjected to sampling bias, and in such cases, it is essential to perform corrections for orientation, truncation, censoring, and size biases.

As a maximum likelihood estimator, the circular estimator method eliminates these sampling biases but only provides information on fracture density, intensity, and mean length, and not on other parameters (e.g., orientation, aperture, or length of individual fractures). The analysis of the two natural fracture networks using these three sampling methods resulted in different fracture characteristics (Table 3), which emphasizes the necessity of a review concerning (1) the minimum required number of measurements and (2) the influence of censored fractures on the estimates of fracture network parameters.

Bonnet et al. (2001) provided a minimum number of measurements required to evaluate the exponent of a power-law fracture length distribution. Similarly, Priest (1993) suggested a minimum number of fractures a sampling area should contain to properly characterize fracture network parameters. Despite these studies providing some basic guidelines, a universally applicable minimum number is probably impossible to obtain because the required number of samples depends on the studied fracture network itself. In this study, we provide a required minimum number for simple fracture networks with power-law length distributions. The power-law exponents used to generate the AFNs represent those commonly reported. For other length distributions, complex fracture networks, or complex sampling area geometries, more fracture lengths should be measured. Although the numbers presented below are not universally applicable, they allow a better estimate on the number of measurements necessary to adequately capture fracture statistics. Our results indicate that the required minimum number of length measurements to define a power-law distribution is approximately 225 for scanline sampling and approximately 110 for window sampling. Note that the size of a sampling area and, therefore, the fracture density, does not directly influence the definition of a length distribution. However, a small sampling area may cause more fractures to be censored, which would lead to a more complex fracture network. For the application of the circular estimator method, we found that approximately 860 fractures should be present in a sampling area to always sample a minimum of 30 fracture endpoints. This minimum number depends on the radius of the circular scanline and decreases for larger radii.

For all three sampling methods, the uncertainty increases with the percentage of censored fractures. The AFNs used in this study are simple. Natural examples, like the ones analyzed here, are commonly much more complex. Hence, it is likely that more fractures are censored. However, because we use percentages of censored fractures, the approach to evaluate the uncertainty is also applicable to natural fracture networks.

The window sampling method provides results with the lowest uncertainty for all network parameters, except for fracture intensity. The reason for this high uncertainty can be explained by the definition of fracture intensity (Table 2) and the approach we used to elaborate the uncertainty caused by censoring bias (Figure 7). Note that fracture intensity can be described as the product of fracture density and mean length (equation 9). If, in a sampling area, both fracture density and mean length are overestimated, then fracture intensity is even more so.

Both the required minimum number of measurements and the uncertainty caused by censoring bias indicate that the window sampling method is the most suitable for the evaluation of the studied natural fracture networks. Table 6 summarizes the measured fracture network parameters and their uncertainty, based on the evaluation in Figure 8.

The uncertainty caused by censoring bias is rather low for the analysis of the lineaments from the satellite image of the Jabal Akhdar dome (Figure 3; Holland et al., 2009a). However, it is also important to consider the resolution limitations of satellite images, which causes a significant truncation bias. For example, LeGarzic et al. (2011) investigated the extensional fracture systems in the Proterozoic basement of Yemen at different scales from multikilometric satellite imagery to 10-m (33-ft) field observations, with length data covering more than three orders of magnitude. The combined multiscale analysis of several thousands of fracture lengths follows a power-law distribution with an exponent of $E = 1.8$. However,

fracture lengths investigated at individual scales were found to follow varying distributions. Truncation bias might be an explanation for the deviation of the length distributions from a power law at individual resolution scales. Hence, correcting the fracture length data for this sampling bias could result in the attainment of distributions closer to the real one.

The results evaluated for the second natural fracture network (Craghouse Park, United Kingdom; Figure 4; Nirex, 1997a) illustrate the high uncertainty of fracture characteristics calculated for such a small outcrop (Table 6). For the power-law exponent, we obtained a value of $E = 2.17$. However, because 30% of the fractures are censored, the potential true value ranges between 1.69 and 2.65, which covers approximately 70% of the values reported by Bonnet et al. (2001). Limitations in the number of measured fractures, the extent of the sampling area, and a high percentage of censored fractures are typical for such small outcrops. However, such outcrops are commonly the only option for the characterization of subsurface fracture networks. For example, Manda and Mabee (2010) sampled between 5 and 76 fractures for two different sets, with 69% or more censored fractures for one of the sets. Although Weiss (2008) considered every outcrop in his study area, he also encountered the problem of having a low number of measurements with a high percentage of censored fractures. A cross-correlation with borehole data could improve the characterization of the subsurface fracture network.

## CONCLUSIONS

The characterization of fracture networks at outcrops can provide essential information for subsurface reservoir models. We present a review on the application of the scanline sampling, window sampling, and circular estimator methods; their governing equations; and a summary of several techniques to correct for sampling bias. In addition, a set of equations and assumptions allows one to compare the results of these sampling methods and to extrapolate these parameters for 3-D fracture networks.

Furthermore, the required minimum number of measurements was evaluated. For the scanline sampling method, approximately 225 measurements are required to define the power-law length distribution, whereas the window sampling requires approximately 110 measurements. These numbers apply to fracture networks that are similar to the AFNs used here. Additional measurements should be considered for the characterization of more complicated fracture network settings. For the application of the circular estimator method, with a radius equal to one-tenth of sampling area extent and assuring a minimum of 30 sampled endpoints, at least 860 fractures should be present in the sampling area. The required minimum number for this method can be reduced by applying a larger radius. If (or how) different radii affect the accuracy of the results should be a topic of future studies.

Uncertainty caused by censored fractures can have large implications for simulations designed to understand the flow behavior of fractured reservoirs. By evaluating the influence of censored fractures on estimates of fracture network parameters, we found that an increasing percentage of censored fractures obviously causes an increase in the difference between measured and true values. Here, the window sampling method provides results with the lowest uncertainty, except for estimates of fracture intensity. To determine intensity, the circular estimator method appears the least sensitive method.

By analyzing the results from a window sampling applied to an outcrop at Craghouse Park (United Kingdom), we found that already 30% of the censored fractures cause a significant uncertainty. However, such small outcrops are commonly all we have to factor into subsurface fracture networks. Therefore, a cross-correlation of data from the analysis of boreholes and outcrops may significantly improve our understanding of the subsurface. Finally, if possible, more than one outcrop or borehole should be analyzed.

## REFERENCES CITED

Barthélémy, J.-F., M. L. E. Guiton, and J.-M. Daniel, 2009, Estimates of fracture density and uncertainties from well data: International Journal of Rock Mechanics and Mining

Sciences, v. 46, p. 590–603, doi:10.1016/j.ijrmms.2008.08.003.
Barton, N., and E. F. de Quadros, 1997, Joint aperture and roughness in the prediction of flow and groutability of rock masses: International Journal of Rock Mechanics and Mining Sciences, v. 34., doi:10.1016/S1365-1609(97)00081-6.
Becker, M. W., 2006, Potential for satellite remote sensing of ground water: Ground Water, v. 44, p. 306–318, doi:10.1111/j.1745-6584.2005.00123.x.
Belayneh, M. W., S. K. Matthäi, M. J. Blunt, and S. F. Rogers, 2009, Comparison of deterministic with stochastic fracture models in water-flooding numerical simulations: AAPG Bulletin, v. 93, p. 1633–1648, doi:10.1306/07220909031.
Berkowitz, B., 2002, Characterizing flow and transport in fractured geological media: A review: Advances in Water Resources, v. 25, p. 861–884, doi:10.1016/S0309-1708(02)00042-8.
Blum, P., R. Mackay, M. S. Riley, and J. L. Knight, 2005, Performance assessment of a nuclear waste repository: Upscaling coupled hydromechanical properties for far-field transport analysis: Journal of Rock Mechanics and Mining Sciences, v. 42, p. 781–792, doi:10.1016/j.ijrmms.2005.03.015.
Blum, P., R. Mackay, and M. S. Riley, 2007, Coupled hydromechanical modelling of flow in fractured rock, *in* J. M. Sharp and J. Krasny, eds., Groundwater in fractured rocks: International Association of Hydrogeologists Selected Paper Series 9, p. 567–574.
Blum, P., R. Mackay, and M. S. Riley, 2009, Stochastic simulations of regional scale advective transport in fractured rock masses using block upscaled hydromechanical rock property data: Journal of Hydrology, v. 369, p. 318–325, doi:10.1016/j.jhydrol.2009.02.009.
Bonnet, E., O. Bour, N. E. Odling, P. Davy, I. Main, P. Cowie, and B. Berkowitz, 2001, Scaling of fracture systems in geological media: Reviews of Geophysics, v. 39, p. 347–383, doi:10.1029/1999RG000074.
Bons, P. D., J. Arnold, M. A. Elburg, J. Kalda, A. Soesoo, and B. P. van Milligen, 2004, Melt extraction and accumulation from partially molten rocks: Lithos, v. 78, p. 25–42, doi:10.1016/j.lithos.2004.04.041.
Bons, P. D., M. A. Elburg, and E. Gomez-Rivas, 2012, A review of the formation of tectonic veins and their microstructures: Journal of Structural Geology, v. 43, p. 33–62, doi:10.1016/j.jsg.2012.07.005.
Bour, O., P. Davy, C. Darcy, and N. Odling, 2002, A statistical model for fracture network geometry, with validation on a multiscale mapping of joint network (Hornelen Basin, Norway): Journal of Geophysical Research, v. 107, p. ETG4-1-ETG4-12, doi:10.1029/2001JB000176.
Castaing, C., A. Genter, B. Bourgine, J. P. Chilès, J. Wendling, and P. Siegel, 2002, Taking into account the complexity of natural fracture systems in reservoir single-phase flow modelling: Journal of Hydrology, v. 266, p. 83–98, doi:10.1016/S0022-1694(02)00114-2.
Cruden, D. M., 1977, Describing the size of discontinuities: International Journal of Rock Mechanics and Mining Sciences Geomechanical Abstracts, v. 14, p. 133–137, doi:10.1016/0148-9062(77)90004-3.
Darcel, C., O. Bour, and P. Davy, 2003, Stereological analysis of fractal fracture networks: Journal of Geophysical Research, v. 108, p. 1–14, doi:10.1029/2002JB002091.
Davy, P., 1993, On the frequency-length distribution of the San Andreas fault system: Journal of Geophysical Research, v. 98, p. 12,141–12,151, doi:10.1029/93JB00372.
Dershowitz, W. S., 1984, Rock joint systems: Ph.D. dissertation, Massachusetts Institute of Technology, Cambridge, Massachusetts, 918 p.
Dershowitz, W. S., and H. H. Einstein, 1988, Characterizing rock joint geometry with joint system models: Rock Mechanics and Rock Engineering, v. 21, p. 21–51, doi:10.1007/BF01019674.
Einstein, H. H., and G. B. Baecher, 1983, Probabilistic and statistical methods in engineering geology: Rock Mechanics and Rock Engineering, v. 16, p. 39–72, doi:10.1007/BF01030217.
Fouché, O., and J. Diebolt, 2004, Describing the geometry of 3-D fracture systems by correcting for linear sampling bias: Mathematical Geology, v. 36, p. 33–63, doi:10.1023/B:MATG.0000016229.37309.fd.
Guerriero, V., S. Vitale, S. Ciarcia, and S. Mazzoli, 2011, Improved statistical multiscale analysis of fractured reservoir analogues: Tectonophysics, v. 504, p. 14–24, doi:10.1016/j.tecto.2011.01.003.
Hatton, C. G., I. G. Main, and P. G. Meredith, 1993, A comparison of seismic and structural measurements of fractal dimension during tensile subcritical crack growth: Journal of Structural Geology, v. 15, p. 1485–1495, doi:10.1016/0191-8141(93)90008-X.
Hilgers, C., D. L. Kirschner, J.-P. Breton, and J. L. Urai, 2006, Fracture sealing and fluid overpressures in limestones of the Jabal Akhdar dome, Oman Mountains: Geofluids, v. 6, p 168–184, doi:10.1111/j.1468-8123.2006.00141.x.
Holland, M., N. Saxena, and J. L. Urai, 2009a, Evolution of fractures in a highly dynamic thermal hydraulic, and mechanical system: (II) Remote sensing fracture analysis, Jabal Shams, Oman Mountains: GeoArabia, v. 14, p. 163–194.
Holland, M., J. L. Urai, P. Muchez, and E. J. M. Willemse, 2009b, Evolution of fractures in a highly dynamic, thermal, hydraulic, and mechanical system: (I) Field observations in Mesozoic carbonates, Jabal Shams, Oman Mountains: GeoArabia, v. 14, p. 57–110.
Hudson, J. A., and S. D. Priest, 1983, Discontinuity frequency in rock masses: International Journal of Rock Mechanics and Mining Sciences and Geomechanical Abstracts, v. 20, p. 73–89, doi:10.1016/0148-9062(83)90329-7.
Jackson, C. P., A. R. Hoch, and S. Todman, 2000, Self-consistency of heterogeneous continuum porous medium representation of fractured medium: Water Resources Research, v. 36, p. 189–202, doi:10.1029/1999WR900249.
Jing, L., and O. Stephansson, 2007, The basics of fracture system characterization: Field mapping and stochastic simulations: Developments in Geotechnical Engineering, v. 85, p. 147–177, doi:10.1016/S0165-1250(07)85005-X.
Koike, K., S. Nagano, and M. Ohmi, 1995, Lineament analysis of satellite images using a segment tracing algorithm

(STA): Computers and Geosciences, v. 21, p. 1091–1104, doi:10.1016/0098-3004(95)00042-7.
Kulatilake, P. H. S. W., and T. H. Wu, 1984, The density of discontinuity traces in sampling windows (technical note): International Journal of Rock Mechanics and Mining Sciences and Geomechanical Abstracts, v. 21, p. 345–347, doi:10.1016/0148-9062(84)90367-X.
Lacazette, A., 1991, A new stereographic technique for the reduction of scanline survey data of geologic features: Computers and Geosciences, v. 17, p. 445–463, doi:10.1016/0098-3004(91)90051-E.
LaPointe, P. R., 2002, Derivation of parent population statistics from trace length measurements of fractal populations: International Journal of Rock Mechanics and Mining Sciences, v. 39, p. 381–388, doi:10.1016/S1365-1609(02)00021-7.
LaPointe, P. R., and J. A. Hudson, 1985, Characterization and interpretation of rock mass joint patterns: Geological Society of America Special Paper 199, p. 37.
Laubach, S. E., 2003, Practical approaches to identifying sealed and open fractures: AAPG Bulletin, v. 87, no. 4, p. 561–579, doi:10.1306/11060201106.
Laubach, S. E., and M. E. Ward, 2006, Diagenesis in porosity evolution of opening-mode fractures, Middle Triassic to Lower Jurassic La Boca Formation, NE Mexico: Tectonophysics, v. 419, p. 75–97, doi:10.1016/j.tecto.2006.03.020.
Laubach, S. E., J. E. Olson, and M. R. Gross, 2009, Mechanical and fracture stratigraphy: AAPG Bulletin, v. 93, p. 1413–1426, doi:10.1306/07270909094.
Lee, C.-H., and I. Farmer, 1993, Fluid flow in discontinuous rock: London, United Kingdom, Chapman & Hall, 169 p.
LeGarzic, E., T. de L'Hamaide, M. Diraison, Y. Géraud, J. Sausse, M. de Urreiztieta, B. Hauville, and J.-M. Champanhet, 2011, Scaling and geometric properties of extensional fracture systems in the Proterozoic basement of Yemen: Tectonic interpretation and fluid flow implications: Journal of Structural Geology, v. 33, p. 519–536, doi:10.1016/j.jsg.2011.01.012.
Llewellin, E. W., 2010, LBflow: An extensible lattice Boltzmann framework for the simulation of geophysical flows: Part I. Theory and implementation: Computers and Geosciences, v. 36, p. 115–122, doi:10.1016/j.cageo.2009.08.004.
Loague, K., and R. E. Green, 1991, Statistical and graphical methods for evaluating solute transport models: Overview and application: Journal of Contaminant Hydrology, v. 7, p. 51–73, doi:10.1016/0169-7722(91)90038-3.
Long, J. C. S., J. S. Remer, C. R. Wilson, and P. A. Witherspoon, 1982, Porous media equivalents for networks of discontinuous fractures: Water Resources Research, v. 18, p. 645–658, doi:10.1029/WR018i003p00645.
Lyman, G. J., 2003, Rock fracture mean trace length estimation and confidence interval calculation using maximum likelihood methods: International Journal of Rock Mechanics and Mining Sciences, v. 40, p. 825–832.
Manda, A. K., and S. B. Mabee, 2010, Comparison of three fracture sampling methods for layered rocks: International Journal of Rock Mechanics and Mining Sciences, v. 47, p. 218–226.
Manzocchi, T., J. J. Walsh, and W. R. Bailey, 2009, Population scaling bias in map samples of power-law fault samples: Journal of Structural Geology, v. 31, p. 1612–1626, doi:10.1016/j.jsg.2009.06.004.
Mauldon, M., 1998, Estimating mean fracture trace length and density from observations in convex windows: Rock Mechanics and Rock Engineering, v. 31, p. 201–216, doi:10.1007/s006030050021.
Mauldon, M., W. M. Dunne, and M. B. Rohrbaugh Jr., 2001, Circular scanlines and circular windows: new tools for characterizing the geometry of fracture traces: Journal of Structural Geology, v. 23, p. 247–258, doi:10.1016/S0191-8141(00)00094-8.
Narr, W., 1996, Estimating average fracture spacing in subsurface rock: AAPG Bulletin, v. 80, p. 1565–1586.
National Research Council, 1996, Rock fractures and fluid flow: Contemporary understanding and applications: Washington, D.C., The National Academies Press, 551 p.
Neuman, S. P., 2005, Trends, prospects and challenges in quantifying flow and transport through fractured rocks: Hydrogeology Journal, v. 13, p. 124–147, doi:10.1007/s10040-004-0397-2.
Neuman, S. P., 2008, Multiscale relationship between fracture length, aperture, density and permeability: Geophysical Research Letters, v. 35, p. 1–6.
Nirex, 1997a, The lithological and discontinuity characteristics of the Borrowdale Volcanic Group at the outcrop in the Craghouse Park and Latterbarrow areas: Nirex Report SA/97/029, 452 p.
Nirex, 1997b, Evaluation of heterogeneity and scaling of fractures in the Borrowdale Volcanic Group in the Sellafield area: Nirex Report SA/97/028, 141 p.
Odling, N. E., 1997, Scaling and connectivity of joint systems in sandstones from western Norway: Journal of Structural Geology, v. 19, p. 1257–1271, doi:10.1016/S0191-8141(97)00041-2.
Odling, N. E., et al., 1999, Variations in fracture system geometry and their implications for fluid flow in fractured hydrocarbon reservoirs: Petroleum Geoscience, v. 5, p. 373–384, doi:10.1144/petgeo.5.4.373.
Olson, J. E., 2003, Sublinear scaling of fracture aperture versus length: An exception or the rule?: Journal of Geophysical Research (American Geophysical Union), v. 108, no. B9, p. 2413, doi:10.1029/2001JB000419.
Olson, J. E., and R. A. Schultz, 2011, Comment on "A note on the scaling relations for opening mode fractures in rock" by C.H. Schultz: Journal of Structural Geology, v. 33, p. 1523–1524, doi:10.1016/j.jsg.2011.07.004.
Olson, J. E., S. E. Laubach, and R. H. Lander, 2009, Natural fracture characterization in tight gas sandstones: Integration mechanics and diagenesis: AAPG Bulletin, v. 93, p. 1535–1549, doi:10.1306/08110909100.
Ortega, O. J., and R. A. Marrett, 2000, Prediction of macrofracture properties using microfracture information, Mesaverde Group sandstones, San Juan Basin, New Mexico: Journal of Structural Geology, v. 22, p. 571–588, doi:10.1016/S0191-8141(99)00186-8.
Ortega, O. J., R. A. Marrett, and S. E. Laubach, 2006, A scale-independent approach to fracture intensity and average spacing measurement: AAPG Bulletin, v. 90, p. 193–208, doi:10.1306/08250505059.

Pahl, P. J., 1981, Estimating the mean length of discontinuity traces: International Journal of Rock Mechanics and Mining Sciences and Geomechanics Abstracts, v. 18, p. 221–228.

Pérez-Claros, J. A., P. Palmqvist, and F. Olóriz, 2002, First and second orders of suture complexity in ammonites: A new methodological approach using fractal analysis: Mathematical Geology, v. 34, p. 323–343, doi:10.1023/A:1014847007351.

Philip, Z. G., J. W. Jennings Jr., J. E. Olson, S. E. Laubach, and J. Holder, 2005, Modelling coupled fracture-matrix fluid flow in geomechanically simulated fracture networks: SPE Annual Technical Conference and Exhibition, San Antonio, Texas, September 29–October 2, 2002, accessed April 11, 2013, http://www.onepetro.org/mslib/servlet/onepetropreview?id=00077340, doi:10.2118/77340-MS.

Pickering, G., J. M. Bull, and D. J. Sanderson, 1995, Sampling power-law distributions: Tectonophysics, v. 248, p. 1–20, doi:10.1016/0040-1951(95)00030-Q.

Priest, S. D., 1993, Discontinuity analysis for rock engineering: London, United Kingdom, Chapman & Hall, 473 p.

Priest, S. D., 2004, Determination of discontinuity size distributions from scanline data: Rock Mechanics and Rock Engineering, v. 37, p. 347–368, doi:10.1007/s00603-004-0035-2.

Priest, S. D., and J. A. Hudson, 1981, Estimation of discontinuity spacing and trace length using scanline surveys: International Journal of Rock Mechanics and Mining Sciences and Geomechanics Abstracts, v. 18, p. 183–197.

Renshaw, C. E., J. S. Dadakis, and S. R. Brown, 2000, Measuring fracture apertures: A comparison of methods: Geophysical Research Letters, v. 27, p. 289–292, doi:10.1029/1999GL008384.

Riley, M. S., 2005, Fracture trace length and number distributions from fracture mapping: Journal of Geophysical Research, v. 110, B08414, 16 p., doi:10.1029/2004JB003164.

Rohrbaugh, M. B. Jr., W. M. Dunne, and M. Mauldon, 2002, Estimating fracture trace intensity, density and mean length using circular scanlines and windows: AAPG Bulletin, v. 86, p. 2089–2104.

Roy, A., E. Perfect, W. M. Dunne, and L. D. Mckay, 2007, Fractal characterization of fracture networks: An improved box-counting technique: Journal of Geophysical Research, v. 112, B12201, 9 p., doi:10.1029/2006JB004582.

Scholz, C. H., 2010, A note on the scaling relations for opening mode fractures in rock: Journal of Structural Geology, v. 32, p. 1485–1487, doi:10.1016/j.jsg.2010.09.007.

Terzaghi, R. D., 1965, Sources of error in joint surveys: Géotechnique, v. 13, p. 287–304.

Tóth, T. M., 2010, Determination of geometric parameters of fracture networks using 1-D data: Journal of Structural Geology, v. 32, p. 1271–1278.

Tóth, T. M., and I. Vass, 2011, Relationship between the geometric parameters of rock fractures, the size of percolation clusters and REV: Mathematical Geosciences, v. 43, p. 75–97.

Toublanc, A., S. Renaud, J. E. Sylte, C. K. Clausen, T. Eiben, and G. Nadland, 2005, Ekofisk field: Fracture permeability evaluation and implementation in the flow model: Petroleum Geoscience, v. 11, p. 321–330, doi:10.1144/1354-079304-622.

Weiss, M., 2008, Techniques for estimating fracture size: A comparison of methods: International Journal of Rock Mechanics and Mining Sciences, v. 45, p. 460–466.

Wu, H., and D. D. Pollard, 1995, An experimental study of the relationship between joint spacing and layer thickness: Journal of Structural Geology, v. 17, p. 887–905, doi:10.1016/0191-8141(94)00099-L.

Zeeb, C., D. Göckus, P. Bons, H. Al Ajmi, R. Rausch, and P. Blum, 2010, Fracture flow modelling based on satellite images of the Wajid sandstone, Saudi Arabia: Hydrogeology Journal, v. 18, p. 1699–1712, doi:10.1007/s10040-010-0609-x.

Zhang, L., and H. H. Einstein, 1998, Estimating the mean trace length of rock discontinuities: Rock Mechanics and Rock Engineering, v. 31, no. 4, p. 217–235, doi:10.1007/s006030050022.

Zhang, L., and H. H. Einstein, 2000, Estimating the intensity of rock discontinuities: International Journal of Rock Mechanics and Mining Sciences, v. 37, p. 819–837.